Chemical Engineering & Technology

Chemical & Engineering Technology

REVIEW ARTICLE OPEN ACCESS

Optimizing Drying Parameters for Crack-Free Catalyst Layers in PEM Fuel Cell Production

Nadine Zimmerer | Philipp Quarz | Linus Janning | Philip Scharfer | Wilhelm Schabel

Karlsruhe Institute of Technology (KIT), Thin Film Technology (TFT), Karlsruhe, Germany

Correspondence: Nadine Zimmerer (nadine.zimmerer@kit.edu)

Received: 4 June 2025 | **Revised:** 24 February 2026 | **Accepted:** 26 February 2026

Keywords: catalyst layer production | crack formation | drying | heat and mass transfer coefficients | relative humidity | temperature

ABSTRACT

The selection of drying parameters critically affects final product properties in many applications, yet remains insufficiently explored for catalyst layer fabrication in polymer electrolyte membrane fuel cells and electrolyzers. During catalyst-coated membrane production, drying conditions strongly influence the macro- and microstructure of porous catalyst layers. Crack formation, which may occur during processing as well as operation, is a key factor limiting system lifetime. Given the wide range of commercial materials and ongoing material development, a mechanistic understanding of crack formation and particularly its control through process parameters rather than ink modification is essential. This study investigates the influence of temperature, airflow, and drying air preloading on crack area and morphology. Through a systematic control of drying parameters, crack-free catalyst layers are feasible.

1 | Introduction

Fuel cells and electrolyzers enable energy storage and supply through hydrogen conversion without the generation of harmful emissions. These technologies are widely regarded as key technologies for establishing a sustainable and climate-neutral energy infrastructure in alignment with the Sustainable Development Goals (SDGs) of the United Nations [1]. Furthermore, they enhance supply security of renewable energy sources and contribute substantially to the decarbonization of energy-intensive sectors. Owing to their high power density, low operation temperatures, and dynamic operating capability, polymer electrolyte membrane (PEM) systems represent a promising technology for both stationary and mobile applications [2, 3].

The central component, in which the energy-converting redox reactions take place, is the catalyst-coated membrane (CCM). The fabrication of CCMs for PEM fuel cells and electrolyzers involves three fundamental processing steps: (i) the formulation and processing of a catalyst ink, (ii) the application of this ink onto a suitable substrate, and (iii) the drying of the wet film to develop a porous catalyst layer, which is important for electrochemical performance. Each of these sub-processes has been widely studied in literature [4–18].

A catalyst ink consists of catalyst particles, an ionomer—which acts both as a binder and for proton conduction in the later catalyst layer—and different solvents. Widely used solvent systems include binary or ternary mixtures of alcohol(s)

Abbreviations: EL, electrolyzer; EW, Equivalent Weight; FC, fuel cell; I/C, Ionomer to carbon ratio; *P*, 1-propanol; PEM, polymer electrolyte membrane; PTFE, polytetrafluorethylen, trade name Teflon; RH, relative humidity; W, water.

and water. The selection of the solvent system governs the interactions between the ionomer and catalyst particles, thereby influencing the micro- and macrostructure of the final catalyst layer [4, 13, 15, 19–23].

In addition, the solvent removal during CCM processing also determines the formation of the microstructure in the functional layer. The drying process is dominated by thermodynamics as well as heat and mass transfer mechanisms of the solvent (mixture) evaporation [24, 25]. These mechanisms are strongly influenced by the applied drying conditions. Therefore, tailoring these parameters is widely employed in various industrial applications, for example, in life science products and in battery electrode processing, to obtain desired material properties [26–30]. This study uses this approach to experimentally demonstrate how targeted control of drying parameters can mitigate or even prevent cracking in catalyst layers for PEM fuel cells and electrolyzers. Although some studies suggest that cracks may enhance reactant mass transport during operation [31], the prevailing consensus in the literature agrees that crack formation negatively impacts the charge transfer processes and the lifetime of PEM systems [19, 32].

Despite the importance of catalyst layer integrity, the mechanisms underlying cracking remain insufficiently understood. Although numerous studies have investigated the influence of ink components (catalyst [33, 34], ionomer content [22, 35], solvent [10, 36, 37], and additives [5, 18]), comparatively little attention has been directed towards the impact of processing parameters during the fabrication of catalyst layers. Given the wide variety of commercially available materials and the continuous development of novel material systems, achieving a mechanistic understanding for controlling crack formation solely through the adjustment of process parameters—without modifying the material composition—would provide a powerful and practical strategy for optimizing existing fabrication routes and extending device lifetime.

1.1 | Microstructure Formation of Porous Layers

During the drying of catalyst layers in PEM systems, microstructural evolution is described using a sequence of distinct stages (Figure 1). This framework, previously established for various porous material systems [24, 27, 38], is extended to include the onset of crack formation, highlighting the critical processing window.

In the first drying period, as the solvents evaporate, the film shrinks and the particles approach each other (a). This phase ends when the particles can no longer approach each other (end of film shrinkage, EOFS) and a porous network with solvent-filled pores has formed (b). Subsequently, solvent evaporation proceeds from the pores of the capillary network. The first cracks become observable (c). Crack formation arises when the drying-induced stresses exceed the mechanical stability of the catalyst layer. First experimentally conducted studies in our group indicate that the beginning of cracking coincides with the end of film shrinkage for catalyst films. The film continues drying, and cracks are propagating through the layer until the film drying finishes (d) [24, 27, 38, 39].

1.2 | Crack Formation in Catalyst Layers

When internal stresses exceed the mechanical stability of the coating, new surfaces in the form of cracks are created to relieve tension. The mechanical properties of the layer are primarily determined by the materials, their composition and their interactions (particle and ionomer (self)interactions), and the overall film thickness [16, 40, 41]. Under identical processing conditions, thicker layers exhibit a higher propensity for crack formation.

Stress accumulation in drying coatings is predominantly attributed to tensile stresses induced by capillary pressure and thus forces within the porous network and differential drying rates between the film surface and its bulk [36, 42, 43]. The cracking is further influenced by heterogeneities in the catalyst ink (e.g., agglomerates) and the applied film (e.g., voids, bubbles), as well as by weak interactions between catalyst particles and ionomer [32, 36]. Additionally, the process conditions, such as the drying conditions, play a critical role in crack initiation and propagation. With variations in the drying rates, significantly impacts on stress development and cracking in catalyst layers are observed [32, 36].

1.3 | Influence of Drying Parameters on Crack Formation in Catalyst Films

The drying process and the drying rate are determined by the employed convective drying parameters, including drying air temperature, heat and mass transfer coefficients, and the initial moisture content of the drying air (relative humidity, RH) or other air preloaded with solvents. Higher drying rates induce rapid dimensional changes within the drying film and reduce the timescale for stress relaxation. Crack formation is initiated when local stress levels reach critical values [40].

Aside from that, the drying parameters significantly influence the (selective) evaporation of the ink solvents. Selective evaporation describes the relative enrichment or depletion of one solvent during drying [17, 44]. Previous studies conducted by the authors have experimentally and analytically demonstrated selectivity during drying of catalyst ink with a commonly employed 1-propanol/water solvent system [17, 45, 46]. Similarly, Scheepers et al. [16] have shown time-resolved concentrations profiles of drying carbon inks with different initial 1-propanol/water concentrations at constant drying conditions. They experimentally observed solvent accumulation and depletion effects during drying using Fourier transform infrared (FTIR) spectroscopy.

The selectivity of solvent evaporation is anticipated to exert a significant impact on the mechanical properties of the catalyst film. Various studies on Nafion solutions have demonstrated that the composition of the alcohol/water solvent system strongly influences the resulting ionomer morphology [4, 19, 21, 22, 47]. Nafion tends to form large, entangled clusters in alcohol-rich solvent systems and rod-like structures in solvent mixtures with high water concentration [47–49]. The differences in ionomer

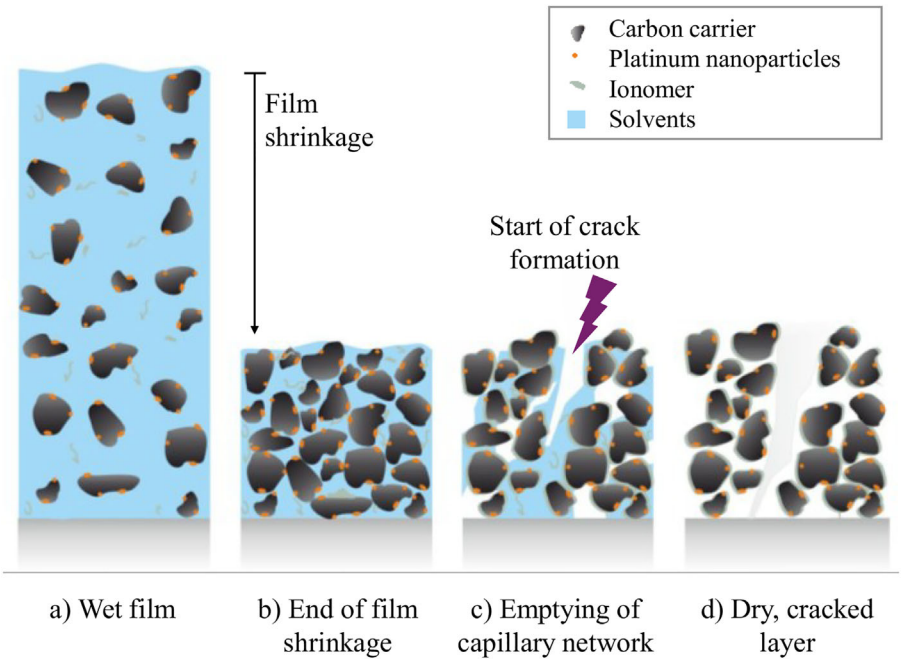

FIGURE 1 | Schematic visualization of the microstructure formation and cracking in catalyst layers during the drying process. Starting with the wet film (a), the film shrinks as drying progresses until the end of film shrinkage (b). Subsequently, solvent removal proceeds predominantly through evaporation from the formed capillary network (c), continuing until the film reaches a dry state (d). Crack formation is expected to occur primarily after the end of film shrinkage, driven by capillary stresses and mechanical constraints.

morphology are likely to effect the interactions with the catalyst particles, the ionomer film on the catalyst particles, and thus the overall mechanical stability of the catalyst layer.

Additionally, stress development within the drying film increases with higher water content due to elevated surface tension, promoting crack formation [40, 50].

The selectivity of the solvent evaporation can be influenced by adjusting the drying parameters [15–17, 19, 44]. A particularly strong influencing factor is the preloading of the drying air [17], as it hinders the evaporation kinetics of the preloaded component and thus leads to an accumulation in the remaining liquid phase.

First investigations into the impact of drying conditions on the microstructure and crack formation in catalyst inks indicate that a lower drying rate, achieved by decreasing the drying temperature or increasing RH, results in the formation of smaller pores within the catalyst layer compared to a higher drying rate [14]. With regard to crack formation, some experiments showed that an increase in drying rate, for example, through elevated drying temperatures, correlates with more cracking [16, 32]. Preloading the drying air with water, on the other hand, reduces the drying rate and the crack formation in catalyst layers [16].

This study systematically investigates the influence of different drying parameters on crack formation in platinum-on-carbon (Pt/C) catalyst layers. For isolating the effects of the individual parameters, the mass transfer coefficient and the drying temperature are independently varied under otherwise constant process conditions to achieve similar drying rates. This approach enables the investigation of the individual drying parameter on crack formation. Mass transfer is linked to heat transfer through the Lewis analogy. An increase in convective heat transfer—for example, by enhancing the airflow velocity—leads to a corresponding rise in the mass transfer coefficient, thereby accelerating solvent evaporation.

In addition, the study explores the effects of preloading the drying air not only with water but also with alcohol, specifically 1-propanol. The objective is to identify critical drying conditions that minimize crack formation and to derive processing guidelines for optimized catalyst layer fabrication.

2 | Experimental Section

2.1 | Ink Formulation and Preparation

The catalyst ink was produced with the platinum-carbon catalyst TEC10EA50E (Tanaka Kikinzoku, Japan). D2020 (20 wt% Nafion polymer with EW = 1000 g mol^{-1} in solution) from Ion Power (USA) was used as the ionomer dispersion in the ink, and an ionomer to carbon (I/C) ratio of 1.0 was set. The solvents used were 1-propanol (Carl Roth GmbH & Co. KG, Germany, purity 99.5%) and ultrapure water. The initial solvent composition was 60 wt% 1-propanol and 40 wt% water. The total solid content of the ink was 10 wt%.

For the ink processing, a dissolver with a ball milling unit (CN10 with APS250, both VMA Getzmann GmbH, Germany) was utilized. In the ball milling unit, yttrium-stabilized zirconium oxide grinding beads with a diameter of 0.6–0.8 mm were added with a volume ratio of 1:1 to the ink volume. The ink was processed for 3 h at 1000 rpm.

TABLE 1 | Drying parameters investigated, including the isothermal film temperature (T) and solvent mass transfer coefficients ($\beta_{p,g}$ for 1-propanol, $\beta_{w,g}$ for water), corresponding to heat transfer coefficient (α), and the resulting average drying rate ($\dot{m}_{mean}$).

T [°C]	$\beta_{p,g}$ (m s^{-1})	$\beta_{w,g}$ (m s^{-1})	α (W m^{-2} K^{-1})	$\dot{m}_{mean}$ (g m^{-2} s^{-1})
25	0.019	0.032	35	1.2
30	0.019	0.032	35	1.7
35	0.019	0.032	35	2.4
25	0.019	0.032	35	1.2
25	0.027	0.046	50	1.8
25	0.041	0.068	75	2.6

Note: Parameters were adjusted to achieve defined drying rates through different process conditions.

The catalyst ink was then applied to a polytetrafluoroethylene (PTFE) substrate (Hightechflon GmbH & Co. KG, Germany) using a ZUA200 doctor blade (Proceq former Zehntner, Switzerland) and dried isothermally. A combination of contact and convective drying is used for isothermal drying conditions. This setup ensures a constant isothermal film temperature during the entire drying process.

2.2 | Drying Setups and Parameters

For investigating the influence of different drying conditions on crack formation, the drying rate was systematically increased by independently varying the mass transfer coefficient and drying temperature. For this, the isothermal drying setup according to [51, 52] was used. The first drying parameter investigated is the isothermal film temperature during drying T, which was systematically increased from 25°C to 35°C in increments of 5°C. These film temperatures correspond to convective air temperatures of 80°C to 145°C in industrial dryers. The convective drying air temperature should not be confused with the film temperature, which is considerably lower due to the equilibrium between convective heat input and evaporative cooling [50]. Using isothermal drying, the film is maintained at film temperature during the entire drying process, ultimately leading to a more precise control of the film drying.

Throughout these experiments, the mass transfer coefficients were constant at 0.019 m s^{-1} for 1-propanol and 0.032 m s^{-1} for water, correlating to a heat transfer coefficient of 35 W m^{-2} K^{-1}. The drying rate is calculated from coupled heat and mass transfer balances of the drying process. Selectivity of evaporation is neglected for simplification. Under these conditions, the averaged, non-selectively calculated drying rate $\dot{m}_{mean}$ during the first drying period increases from 1.0 g m^{-2} s^{-1} at 25°C to 2.1 g m^{-2} s^{-1} at 35°C, effectively doubling the drying rate. A summary of the drying conditions is provided in Table 1. The dew point of the drying air during the convective experiments was $\tau = 4.6$°C. This corresponds to RH (25°C) = 27%.

The second parameter, the mass transfer coefficients of 1-propanol $\beta_{p,g}$ and water $\beta_{w,g}$ and thus the corresponding heat transfer coefficient α, was more than doubled by modify convective flow conditions. Throughout these experiments, the isothermal film temperature was maintained at 25°C. The corresponding drying rates for the applied drying conditions are presented in Table 1.

Lastly, the effect of preloading the drying air, meaning the enrichment of the air with one solvent, was examined. The experiments included air preloadings with water and 1-propanol. In the case of water, this is often referred to as the RH. Preloading the drying air with one solvent inhibits the evaporation of this solvent, leading to its relative accumulation in the liquid phase during drying.

For this, a novel experimental setup for isothermal drying with pre-conditioned air has been developed (see Figure 2). A PTFE substrate, on which the film is coated, is fixed on a heated plate T_{table}, ensuring controlled isothermal drying conditions ($T_{table} = T_{air} = T$). Dry compressed air (dew point $\tau_0 = -16.6$°C) was saturated with the respective solvent using a temperature-controlled saturator. Different saturator temperatures were employed to achieve varying solvent loadings in the drying air. For water saturation, temperatures of 10.5°C and 19.0°C were used, and for 1-propanol, 10.5°C. The saturated air was subsequently heated via a heat exchanger to T_{air} and directed to a drying nozzle to laterally overflow the catalyst films. The experimental setup is enclosed to shield the experiment from external influences. Before starting the experiments, a stabilization period was implemented to allow the air temperature to equilibrate at the target value of $T = 25$ °C. During this phase, the experimental chamber was flushed with preloaded air. This procedure was conducted to establish reproducible conditions for the experiments.

Isothermal drying was conducted at 25°C for water-preloaded air and at 35°C for 1-propanol-preloaded air. With this setup, dew points of 10.2°C (RH ($T = 25$°C) = 39%) and 14.5°C (RH ($T = 25$°C) = 52%) of the drying air humidified with water were measured at the drying nozzle outlet. The differences between the set saturation temperatures and the measured dew points can be attributed to the accuracy and losses of the experimental setup. The preloading of 1-propanol was not measured directly but estimated assuming full saturation at 10.5 °C followed by preheating to 35 °C, resulting in a calculated activity of 20%.

Additionally, a precise determination of flow conditions and the corresponding heat and mass transfer coefficients is complex, as these parameters depend on both the volumetric airflow rate and the distance to the drying nozzle [53]. Therefore, sampling for crack analysis was confined to a region approximately 4–5 cm downstream of the drying nozzle outlet to ensure consistency of the drying parameters. However, the experimental setup is sufficiently applicable to qualitatively assess the influences of solvent preloading on crack formation in catalyst layers.

2.3 | Characterization Methods of the Dry Catalyst Layer

The dried catalyst layers were characterized using the layer thicknesses and optical methods for crack detection. The layer

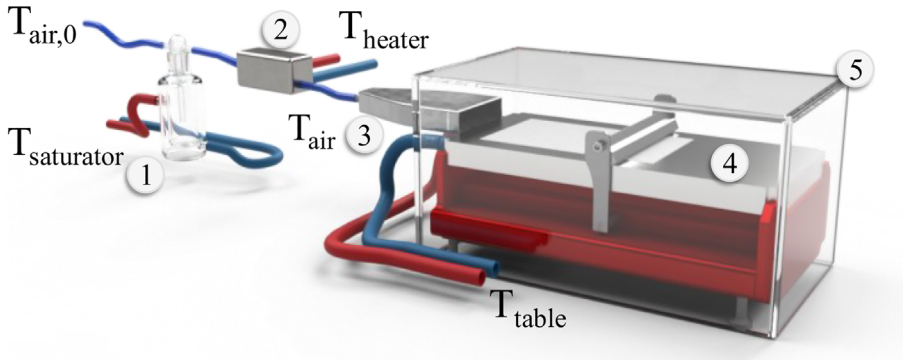

FIGURE 2 | Schematic illustration of the preloading setup with isothermal drying conditions and lateral air overflow. The setup consists of the temperature-controlled saturator with water or 1-propanol (1), the heat exchanger for air heating (2), the drying nozzle (3), the temperature-controlled coating plate (4), and the Plexiglass enclosure (5) for shielding the experiment from external influences. The air ($T_{air,0}$, τ_0) is first saturated, then heated (T_{air}, τ), and subsequently led to the drying nozzle.

thickness was measured using an ID-H0530 gauge (Mitutoyo, Japan). As the layer height is a critical parameter influencing crack formation, the objective is to compare layers with similar thicknesses within standard deviations. Additionally, microscope images in backlight illumination were captured using a VHX-7000 microscope (Keyence, Japan) at 100× magnification. Through the technique of microscope stitching, wherein individual microscope images are aligned to cover a larger representative area, a region of 2 × 2 cm^2 was analyzed. The acquired images are subsequently divided into four quadrants for individual analysis of crack area and number using an in-house AI-assisted tool. Arising standard deviations emerge from spatial heterogeneities of the crack patterns in the analyzed image sections, as microscope settings and image processing were held constant during the analyses.

3 | Results and Discussion

3.1 | Increasing Drying Rate With Drying Temperature or Overflow Conditions

Key process-related parameters influencing convective drying and the associated drying rate include the drying temperature and the flow dynamics, the latter characterized by the heat and mass transfer coefficient. First, the drying rate is systematically increased by adjusting either the film temperature during drying or the heat and mass transfer coefficient. By adjusting these two drying parameters, the drying rate is first increased by 50% and 100% in the second step (Table 1).

Figure 3 shows representative sections of the dried catalyst layers using backlight illumination. A quantitative analysis of the area and number of cracks is plotted in Figure 5. In this investigation, the isothermal film temperature during drying was systematically increased from 25°C to 30°C and subsequently to 35°C, whereas the heat and mass transfer coefficient was maintained constant at $\beta_{p,g}$ = 0.019 m s^{-1}, $\beta_{w,g}$ = 0.032 m s^{-1}, and thus α = 35 W m^{-2} K^{-1}. With backlight illumination, cracks appear as white regions, whereas the intact catalyst layer is black. Given the strong dependance between crack formation and layer thickness, it is important to ensure similar thicknesses to isolate the effects of drying parameters on crack formation. The film thicknesses, measured from left to right, are 9.0 ± 0.6, 9.9 ± 1.7, and 9.7 ± 1.3 µm.

The catalyst layer dried at 25°C serves as the reference for subsequent variations in drying parameters. Under these conditions, isolated cracks are observed. Most of the cracks have an I-, Y-, or T-shaped structure with only few branches. With increasing drying temperature, cracks become smaller and the crack structures thinner. The crack morphologies shift towards more rounded U-shapes, although Y- and T-shaped patterns persist. No preferential orientation of the cracks can be recognized in the catalyst layers.

In the second part of this study, the mass transport coefficients, and accordingly the heat transfer coefficient, were systematically increased to achieve drying rates comparable to those obtained in the temperature variation (Table 1). Specifically, isothermal drying was conducted at a constant film temperature of 25°C, with mass transfer coefficients of 0.019, 0.027, and 0.041 m s^{-1} for 1-propanol and, respectively, 0.032, 0.046, and 0.068 m s^{-1} for water (Table 1). These correlate to heat transfer coefficients of 35, 50, and 75 W m^{-2} K^{-1} and will hereafter be referred to accordingly. Figure 4 shows representative images of the resulting catalyst layers, acquired using the same imaging methodology as in the previous figure. From left to right, the film thicknesses are 9.0 ± 0.6, 9.9 ± 1.7, and 9.7 ± 1.3 µm. The first image on the left in both Figures 3 and 4 is identical and serves as the baseline for the comparative analysis.

An increase in the heat transfer coefficient, and consequently the drying rate, results in a higher number of cracks within the dry catalyst layers. However, an interconnected crack network does not develop; instead, cracks predominantly remain individually distributed in the catalyst layer. Alongside the increased number of cracks, both the average crack length and the branching of the cracks increase noticeably with higher drying rates. At lower heat and mass transfer coefficients, predominantly I-shaped cracks and only few Y- and T-shaped morphologies are observed. However, with increasing drying rates, the degree of crack branching becomes more pronounced, and most cracks show multi-branched forms. The total crack area appears to

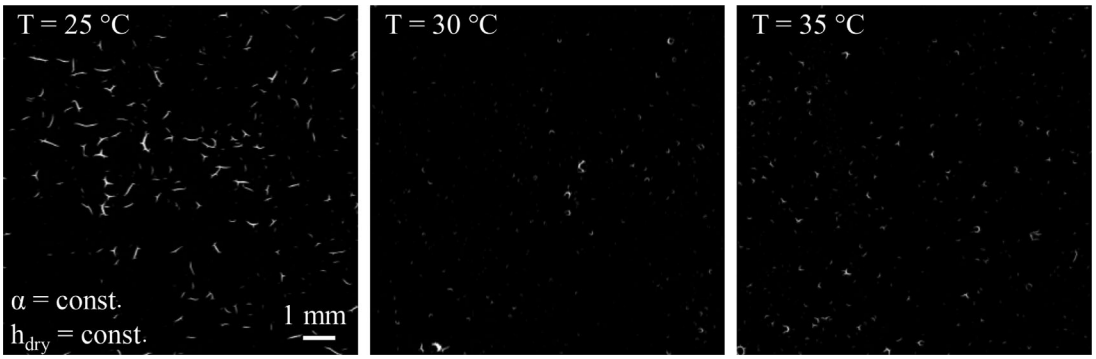

FIGURE 3 | Effect of increasing drying temperature on crack formation. Cracks appear white in the representative microscope stitching images of the catalyst layers (1×1 cm^2). From left to right, the isothermal film temperature was increased from 25°C to 30°C and 35°C, corresponding to convective air temperatures of 80–145°C in industrial dryers. Higher drying rates are achieved with increasing temperature, whereas air flow conditions and layer thickness remain constant.

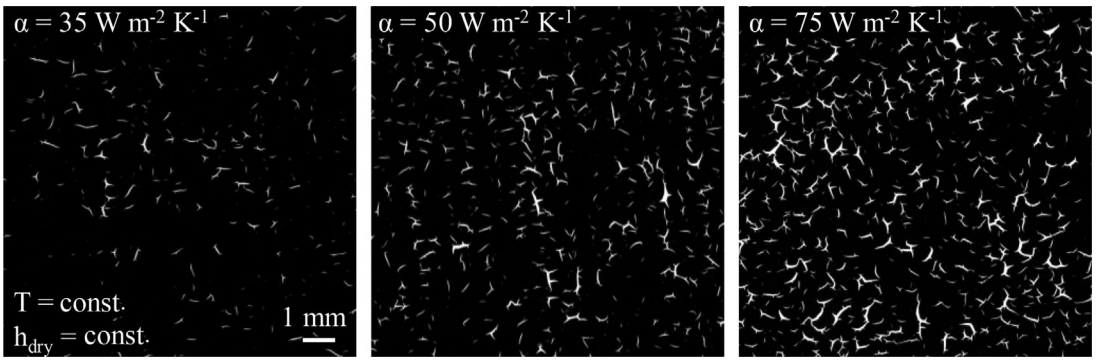

FIGURE 4 | Effect of increasing heat and mass transfer coefficients on cracking. Cracks appear white in the representative microscope stitching images of the catalyst layers (1×1 cm^2). From left to right, air overflow conditions, and consequently the heat and mass transfer coefficients and drying rates, were increased. The mass transfer coefficients of 1-propanol and water were more than doubled and correspond to heat transfer coefficients of 35, 50, and 75 W m^{-2} K^{-1}. The film temperature during drying was kept at 25°C.

expand, indicating greater mechanical stresses during faster solvent evaporation.

Figure 5 presents a comparative analysis of the determined cracked area compared to the total catalyst layer area (Figure 5a) and the number of cracks per cm^2 (Figure 5b) observed in the examined representative images from Figures 3 and 4. The crack analysis data are listed in the Supporting Information Section S2. Here, the effects of increased drying rates induced via two distinct process routes—increased film temperature during drying and adjusted mass transfer coefficients—are evaluated. The drying rates are calculated and averaged over the first drying period neglecting effects of selective evaporation. According to the Lewis analogy, mass transfer coefficients are directly correlated to heat transfer coefficients. In the subsequent discussion, the heat transfer coefficient is used as a representative parameter. An overview of the applied drying parameters is provided in Table 1. The combinations of drying parameters are chosen to result in comparable drying rates.

The reference drying rate at an isothermal film temperature during drying of 25°C and a heat transfer coefficient of 35 W m^{-2} K^{-1} is 1.2 g m^{-2} s^{-1}. The drying rate was increased to 1.7 and 1.8 g m^{-2} s^{-1}, achieved either by raising the temperature to 30°C while maintaining α = 35 W m^{-2} K^{-1}, or by increasing the heat transfer coefficient to 50 W m^{-2} K^{-1} at 25°C. A further raise in drying rate to 2.4 and 2.6 g m^{-2} s^{-1} was obtained by the drying parameter combinations of T = 35°C with α = 35 W m^{-2} K^{-1} and α = 75 W m^{-2} K^{-1} at 25°C. These controlled variations enable a systematic comparison of the influence of individual process parameters on the extent of crack formation in representative areas of the catalyst layers (Figures 3 and 4).

An increase in the drying rate through elevation of the heat and mass transfer coefficients leads to a significant rise in both the relative crack area (Figure 5a) and the total number of detected cracks (Figure 5b) within the layers. The relative crack area is defined as the ratio of the total crack area to the total catalyst layer area. At the lowest heat transfer coefficient (35 W m^{-2} K^{-1}), the cracked area accounts for 1.14% ± 0.30% of the total catalyst layer surface. However, upon increasing the drying rate by 40% (50 W m^{-2} K^{-1}), the crack area is 3.49% ± 0.46%. The highest drying rate (2.2 g m^{-2} s^{-1}) results in the most extensive crack formation, with 6.05% ± 0.77% of the surface showing cracks. Furthermore, the total number of detected cracks increases with rising heat transfer coefficients, from 539 ± 41 cm^{-2} at 35 W m^{-2} K^{-1} to 814 ± 45 cm^{-2} at 50 W m^{-2} K^{-1}, and further to 1266 ± 151 cm^{-2} at 75 W m^{-2} K^{-1}.

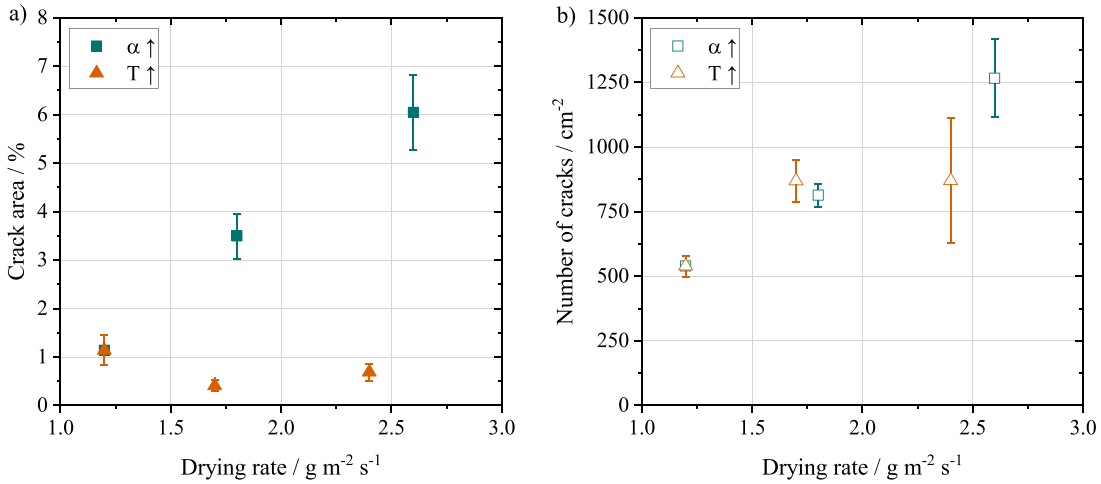

FIGURE 5 | Crack area (a) and number of cracks (b) in representative catalyst layer sections (Figures 3 and 4) dried under varying drying conditions. The effect of increasing isothermal film temperature (25°C, 30°C, 35°C) is shown in orange, whereas the influence of elevated heat transfer coefficient (35, 50, 75 W m^{-2} K^{-1}) is shown in turquoise.

In contrast, coatings dried at comparable drying rates—achieved through elevated isothermal film temperature while maintaining constant mass transfer coefficients—exhibit significantly reduced crack areas. At a drying rate of 1.5 g m^{-2} s^{-1} (and isothermal film temperature during drying of 30°C), the crack area is only 0.41% ± 0.12% of the total analyzed catalyst area. This represents an 8.5-fold decrease compared to coatings dried at similar drying rates with increased heat transfer coefficient. Similarly, at a drying rate of 2.1 g m^{-2} s^{-1} and 35°C, the crack area is reduced by a factor of 8.7.

As the drying rates are calculated from heat and mass transfer balances, they should be considered only as approximations. Nevertheless, beyond the exact drying rate values, the impact of accelerated drying, induced by changes in airflow or temperature, on crack formation in catalyst layers is clearly evident.

When directly comparing the layers dried with increasing isothermal film temperature during drying, the temperature rise only shows a weak correlation with crack formation. Overall, a small reduction in total crack area is observed. The number of detected cracks, however (Figure 5b), increases by approximately 61% with an elevated film temperature of 30°C. Consequently, the average crack is smaller with increasing drying rate. A further increase in the drying rate from 1.5 to 2.1 g m^{-2} s^{-1} does not result in a higher number of cracks; however, it leads to a significantly greater standard deviation, suggesting increased heterogeneity in the stress distribution within the layers. This trend of increased deviations at higher drying rates is also evident under conditions of elevated heat and mass transfer coefficients.

Furthermore, in additional experiments (see Supporting Information Section S3), the observed trend of increasing crack area percentage with higher drying rates (with higher heat and mass transfer coefficients) was also confirmed for other layer thicknesses (approximately 7 µm). Additionally, the slight reduction in crack proportion with increasing film temperature was similarly observed for this layer thickness. Likewise, similar trends associated with the accelerated drying were observed for another ink formulation (see Supporting Information Section S4) with higher water content ($x_{1\text{-Prop}}$ = 18 wt%, x_{Water} = 72 wt%, and x_{soldis} = 10 wt%). Through all experiments, catalyst layers dried with increasing air flow rate consistently exhibit a greater percentage of crack area compared to coatings dried with lower drying rates. The effect of isothermal film temperature during drying remains inconclusive when comparing the two ink formulations, indicating that temperature may also modulate additional phenomena during the ink drying process—such as the selective evaporation of mixture components or the temperature-dependent behavior of the polymer–particle interactions.

Overall, these findings indicate that increasing the drying rate by altering the air flow conditions (and thus the heat and mass transfer coefficients) leads to enhanced crack formation. This aligns with the previous findings from Scheepers et al. [16] that a higher drying rate promotes cracking due to reduced time for stress relief during drying.

However, an increase in film temperature during drying—despite also accelerating the drying rate—exhibited only a minor or even inhibitory effect on crack formation in catalyst layers. The results suggest that catalyst films subjected to elevated temperatures are more effective in absorbing and dissipating internal stresses induced by accelerated drying. This behavior could be attributed to the temperature-dependent properties of the materials, such as those of the Nafion ionomer, which could contribute to greater stress relaxation. Supporting these hypotheses, studies on the thermomechanical behavior of Nafion membranes have shown that below the glass transition temperature, increasing the temperature leads to reduced tensile strength and more effective stress relaxation [54, 55]. However, membrane properties differ from those of ionomers in solution, and temperature ranges investigated in these studies cover a broader spectrum. Systematic investigations of the storage modulus of Nafion solutions and catalyst inks should be focus of future investigations.

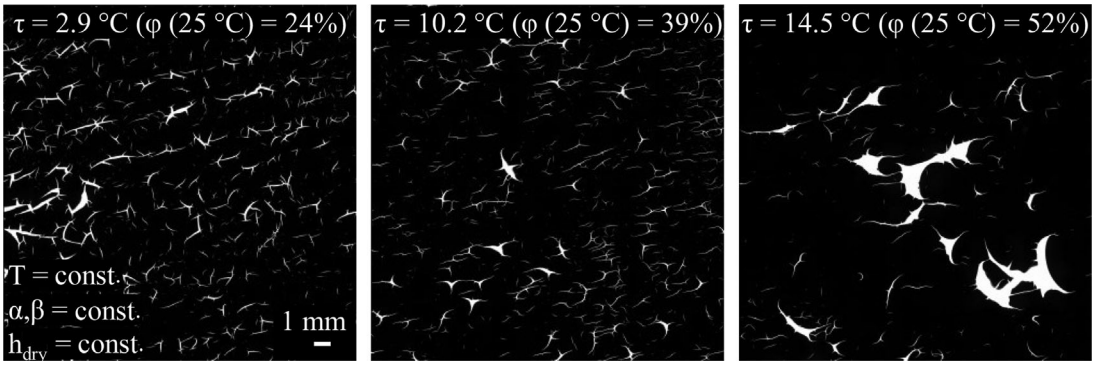

FIGURE 6 | Influence of relative humidity of the drying air on crack formation. Cracks appear white in the representative microscope stitching images ($2 \times 2\ cm^2$). From left to right, air preloading (dew point) was increased from 2.9°C to 10.2°C and 14.5°C. Higher air preloading reduces the drying rate. Film drying was performed using the setup in Figure 2, with drying temperature, overflow conditions, and layer thickness maintain constant.

3.2 | Influence of Preloading the Drying Air With Solvents

Another often underestimated parameter that can significantly influence both the drying rate and the selective evaporation of ink solvents is the preloading of the drying air. Preloading refers to the prior partial saturation of the air with a solvent before the start of the drying process. In most applications, unless the drying air is explicitly conditioned, it inherently contains a certain level of water vapor, commonly referred to as RH. Seasonal variations of the weather and climatic differences cause differences in humidity, which will affect the drying behavior. In Karlsruhe, Germany, annual variations in RH can range from air dew points as low as −0.8°C in winter to as high as 19.1°C in summer (referenced at 25°C, this corresponds to relative humidities of 18% and 70%). In addition, industrial dryers are commonly operated with a partial recirculation of process air to improve energy efficiency. In such configurations, the recirculated air is enriched with the evaporated components of the ink solvents. Preloading the drying air with a solvent of the ink hinders its evaporation, thereby altering the speed and selectivity of the drying process. In the case of catalyst inks for fuel cells and electrolyzers with alcohol-water solvent mixtures, for example, this will influence the solvent composition in the film during drying. Changes in solvent composition can impact the self-assembly and interactions of the solid ink components, including ionomer morphology and ionomer film thickness on catalyst particles and interaction (Section 1.3).

First, the effect of preloading the drying air with water on crack formation in the catalyst layer is evaluated. To ensure controlled experimental conditions, an experimental setup is designed, where the drying parameters (overflow velocity and isothermal temperature) are maintained constant, whereas only the humidity of the drying air is systematically varied (see Figure 2). In the experiments, the isothermal film temperature during drying was set to 25°C. A direct comparison with the preceding experiments (Chapter 3.1) is not feasible, due to differing flow conditions.

Figure 6 shows representative microscope images of catalyst layers dried with different water preloadings. From left to right, the dew point of the drying air is 2.9°C (corresponding to RH = 24% at an air temperature of 25°C), 10.2°C (RH (25°C) = 39%), and 14.5°C (RH (25°C) = 52%). This adjustment enables an increase of more than twofold in the RH. The dry film thicknesses are comparable with 8.0 ± 1.6, 8.4 ± 1.1, and 8.2 ± 0.7 µm (from left to right).

At the investigated RHs and with the examined layer thickness, all catalyst layers show isolated individual cracks rather than a continuous crack network. An increase in humidity leads to a reduction in the number of cracks. At the highest humidity in the drying air ($\tau = 14.5$°C), the cracks are longer and wider. Spalling of the catalyst layer from the substrate can be observed at large crack morphologies, which appears as large white areas in the backlight images. First signs of spalling are also observed when drying with air at $\tau = 10.2$°C. Furthermore, higher humidity, and consequently lower drying rates, results in reduced crack branching.

For a detailed analysis of the crack formation, Figure 7 plots the crack area fraction (left) and the number of cracks per cm^2 (right) against the dew point of the drying air. The RH was increased by more than a factor of two at the extreme conditions ($RH_{\tau = 2.9°C}(25°C) = 24\%$ and $RH_{\tau = 14.5°C}(25°C) = 52\%$).

No clear trend is observed for the percentage of cracked area in the catalyst layers (Figure 7a) as the dew point of the drying air increases. First, the crack area decreases from 5.3% ± 1.2% to 3.4% ± 0.2% with an increase in dew point from τ = 2.9°C to 10.2°C. However, with a further rise in humidity, the catalyst layers show again 4.5% ± 2.0% of cracked area. Notably, the catalyst layers dried at the highest RH show the greatest standard deviations. This can be attributed to the reduction in the number of cracks with increasing humidity (Figure 7b). The fewer but larger cracks at higher air humidities, along with the occurrence of spalling of the catalyst layer from the substrate, result in areas where the catalyst layer is almost intact but also regions where it has nearly completely spalled.

For subsequent processing of the catalyst layers, for example during hot-pressing onto the proton-conducting membrane in CCM fabrication, as well as during operation with respect to system performance and durability, catalyst layers without spalling are expected to be advantageous. These layers were obtained when drying was performed under lower humidity conditions.

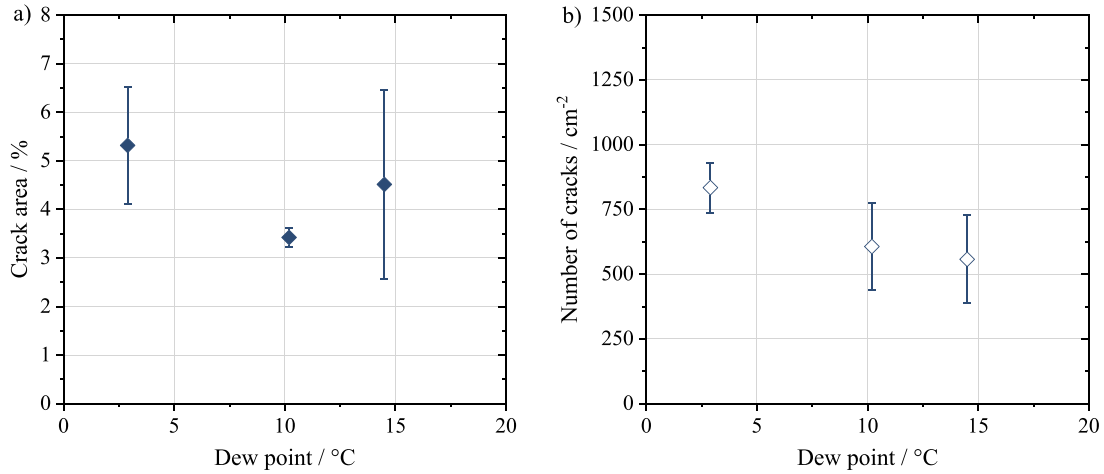

FIGURE 7 | Crack area relative to total layer area (a) and number of cracks (b) in catalyst layers dried isothermally at 25°C with different water preloadings of the drying air (Figure 6). Air dew points of 2.9°C, 10.2°C, and 14.5°C correspond to relative humidities of 24%, 39%, and 52% at 25°C, respectively.

The observed differences in the crack pattern, at constant temperature and overflow conditions but with increasing RH of the drying air, can be attributed to both the reduced drying rate and the selective evaporation of the ink solvents. According to the findings presented in the previous section, a decrease in the drying rate (in this case due to increasing air humidity) results in a reduction in the number of cracks, which is consistent with the observations at water preloading conditions. However, this does not account for the larger size of the cracks and the occurrence of spalling of the layer from the substrate in the vicinity large crack structures. Hence, this could indicate higher stresses during drying. Once cracks form, they tend to propagate and enlarge. A potential explanation can be related to the selective evaporation behavior of the ink solvents under humidified drying conditions. The RH of the drying hinders the evaporation of water during the drying process, causing water to accumulate relatively within the drying catalyst film, whereas 1-propanol preferentially evaporates [25]. Capillary forces, which are closely associated with stress development in the films, are directly proportional to the surface tension of the solvent mixture. Higher water contents in the film will result in higher surface tension of the liquid, ultimately leading to higher stresses during drying [15, 40, 56]. Measured surface tensions for 1-propanol/water mixtures with different concentrations are included in the Supporting Information Section S1 for reference.

As a final step, and to mitigate the previous effect of relative water enrichment, the preloading of the drying air with 1-propanol was investigated. In industrial applications, preloading of the air with both ink solvents exists during operation of a roll-to-roll convection dryer with recirculating air. However, it is essential that all safety regulations for working with and in an alcohol-loaded atmosphere (e.g., explosion protection and exposure dose limits) are strictly followed.

It should also be noted that the experimental setup does not include a vacuum unit to strip the air of the drying chamber prior to the experiments. Therefore, a certain level of preloading of the drying air with water cannot be avoided due to the RH of the surrounding air.

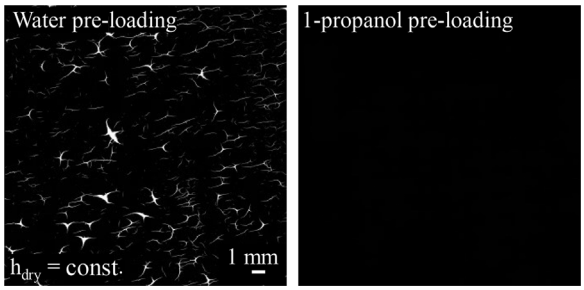

FIGURE 8 | Comparison of crack formation in catalyst layers dried with air preloaded with water and 1-propanol. Cracks appear white in the representative microscope stitching images (2 × 2 cm^2). In both cases, air was first saturated with the solvent at 10.5°C, then heated to 25°C (water) or 35°C (1-propanol). Drying was performed isothermally using combined conductive and convective heat input for drying (Figure 2). Preloading the drying air with 1-propanol results in crack-free catalyst layers at comparable dry film thicknesses of 8.4 ± 1.1 µm (water) and 8.9 ± 1.6 µm (1-propanol).

A comparison of a catalyst layer dried with 1-propanol preloaded air to the previous results is presented in Figure 8. The layer on the left was dried with air with water preloading, whereas the layer on the right was dried with 1-propanol-loaded air. A saturator temperature of 10.5°C (see Figure 2) was applied for drying at both preloading conditions (left and right). Preloading the air with 1-propanol reduces the (non-selectively calculated) drying rate by 35% at otherwise identical drying conditions. To mitigate this reduction in drying rate, the isothermal film temperature during drying was increased to 35°C.

Clear differences are observed when comparing the catalyst layer images. Although preloading the drying air with water results in a cracked catalyst layer, no visible cracks are present in the layer dried at 1-propanol preloading conditions. Detailed microscopy analysis reveals, however, that on average a number of 3 ± 1 cm^{-2} cracks are detected in the analyzed samples of the 1-propanol preloaded drying conditions. This corresponds to a crack area of only 0.0002% ± 0.0001% of the total catalyst area. In contrast,

the layer dried with water-preloaded air exhibited a crack area percentage of 3.4 ± 0.2, and an average number of cracks of 606 cm^{-2} was detected.

This finding highlights the significance of the air preloading and overall the drying (parameters) on the formation of cracks in catalyst layers. In the case of the catalyst ink used here, which has an initial solvent composition of 60 wt% 1-propanol and 40 wt% water, the ink composition during the drying process can be substantially influenced by preloading the drying air with the corresponding solvent. When the drying air is preloaded with 1-propanol, its evaporation is impeded, causing water to evaporate preferentially, whereas 1-propanol accumulates relatively within the drying catalyst film. Conversely, preloading with water results in the opposite effect. Thus, the composition of the catalyst film during the drying process is significantly different in the two studied cases.

Clearly, the enrichment of 1-propanol in the catalyst film is beneficial in terms of crack mitigation. As 1-propanol has a lower surface tension than water, the relative enrichment of 1-propanol in the film reduces the overall surface tension of the liquid. According to Singh and Tirumkudulu [40], this lowers capillary stresses within the porous structure and, consequently, the driving force for crack formation. Additionally, increasing the 1-propanol content in the film influences the ionomer morphology. Nafion tends to form larger, entangled ionomer clusters in propanol-rich solutions. Khandavalli et al. [48] also reported an enhanced viscoelasticity of the ionomer dispersion with higher propanol content. These characteristics are expected to improve the mechanical properties of the drying catalyst film and its ability to dissipate developing stresses. Consequently, the combined effects of reduced drying stresses and enhanced stress-relaxation capacity of the ionomer at higher 1-propanol contents at the critical time for cracking provide a possible explanation for the observed significant reduction of crack formation in catalyst layers.

4 | Conclusion

This study systematically investigates the influence of drying parameters, namely, temperature, convective air flow conditions (heat and mass transfer coefficients), and drying air preloading, on crack formation in Pt/C-based catalyst layers for PEM fuel cells and electrolyzers. The results demonstrate that accelerated drying generally promotes crack formation due to enhanced stress accumulation; however, the crack morphology depends on the drying parameter applied. Increased heat and mass transfer coefficients enlarge the total crack area, whereas elevated film temperatures lead to the formation of smaller cracks in the catalyst film. The preloading of the drying air was identified as the most critical parameter influencing crack formation. Higher air pre-loading with water (RH) resulted in fewer but larger cracks. In contrast, pre-loading the drying air with 1-propanol, while maintaining an identical ink composition, enables the fabrication of crack-free catalyst layers. By providing a systematic evaluation of drying parameters, this work establishes a framework for tailoring crack morphologies in catalyst layers solely through adjusting process parameters. On this basis, subsequent studies should evaluate the impact of critical crack dimensions on cell performance and durability to determine an optimal trade-off between the beneficial and detrimental effects of cracking in catalyst layers.

Nomenclature

Symbols

h_{dry}	Layer thickness of the dry catalyt layer
$\dot{m}_{mean}$	averaged, unselectively calculated drying rate of the first drying period, g m^{-2} s^{-1}
T	Drying temperature
T_{air}	temperature of the convective air, °C
T_{heater}	temperature of the heat exchanger to heat the saturated drying air, °C
$T_{isotherm}$	isothermal film temperature during drying, °C
T_{table}	temperature of the coating table, °C
x_i	mass fraction of ink component *i*, wt%

Greek Variables

α	heat transfer coefficient, W m^{-2} K^{-1}
$\beta_{p,g}$	mass transfer coefficient of 1-propanol in air, m s^{-1}
$\beta_{w,g}$	mass transfer coefficient of water in air, m s^{-1}
τ	drew point of drying air, °C

Author Contributions

Nadine Zimmerer: conceptualization, visualization, methodology, investigation, data curation, validation, original draft preparation, and editing. **Philipp Quarz**: conceptualization, methodology, and reviewing. **Linus Janning**: conceptualization and reviewing. **Philip Scharfer**: reviewing and supervision. **Wilhelm Schabel**: reviewing and supervision.

Acknowledgments

The authors would like to thank Angela Duhatschek, Jonas Risinger, and Tim Schmedding for their aid in conducting the experimental results of the study.

Open access funding enabled and organized by Projekt DEAL.

Funding

The authors have nothing to report.

Conflicts of Interest

The authors declare no conflicts of interest.

Data Availability Statement

The data that support the findings of this study are available in the Supporting Information of this article.

References

1. United Nations, *Transforming Our World: The 2030 Agenda for Sustainable Development* (United Nations,2015).

2. J. Töpler and J. Lehmann, eds., *Wasserstoff und Brennstoffzelle: Technologien und Marktperspektiven* (Springer Berlin Heidelberg, 2017).

3. U. Schelling, *Energietechnik: Systeme Zur Konventionellen und Erneuerbaren Energieumwandlung* (Kompaktwissen für Studium und Beruf, Springer Fachmedien Wiesbaden, 2019).

4. T. T. Ngo, T. L. Yu, and H.-L. Lin, "Influence of the Composition of Isopropyl Alcohol/Water Mixture Solvents in Catalyst Ink Solutions on Proton Exchange Membrane Fuel Cell Performance," *Journal of Power Sources* 225 (2013): 293–303, https://doi.org/10.1016/j.jpowsour.2012.10.055.

5. C. M. Baez-Cotto, J. R. Pfeilsticker, H. Yu, et al., "Impact of Polymer Additives on Crack Mitigation of Rod-Coated Fuel Cell Cathode Catalyst Layers," *Journal of Power Sources* 592 (2024): 233852, https://doi.org/10.1016/j.jpowsour.2023.233852.

6. Y. Guo, F. Pan, W. Chen, et al., "The Controllable Design of Catalyst Inks to Enhance PEMFC Performance: A Review," *Electrochemical Energy Reviews* 4, no. 1 (2021): 67–100, https://doi.org/10.1007/s41918-020-00083-2.

7. M. Wang, J. H. Park, S. Kabir, et al., "Impact of Catalyst Ink Dispersing Methodology on Fuel Cell Performance Using In-Situ X-Ray Scattering," *ACS Applied Energy Materials* 2, no. 9 (2019): 6417–6427, https://doi.org/10.1021/acsaem.9b01037.

8. S. Du, W. Li, H. Wu, P.-Y. Abel Chuang, M. Pan, and P.-C. Sui, "Effects of Ionomer and Dispersion Methods on Rheological Behavior of Proton Exchange Membrane Fuel Cell Catalyst Layer Ink," *International Journal of Hydrogen Energy* 45, no. 53 (2020): 29430–29441, https://doi.org/10.1016/j.ijhydene.2020.07.241.

9. P. Toudret, J.-F. Blachot, M. Heitzmann, and P.-A. Jacques, "Impact of the Cathode Layer Printing Process on the Performance of MEA Integrating PGM Free Catalyst," *Catalysts* 11, no. 6 (2021): 669, https://doi.org/10.3390/catal11060669.

10. A. Therdthianwong, P. Ekdharmasuit, and S. Therdthianwong, "Fabrication and Performance of Membrane Electrode Assembly Prepared by a Catalyst-Coated Membrane Method: Effect of Solvents Used in a Catalyst Ink Mixture," *Energy & Fuels* 24, no. 2 (2010): 1191–1196, https://doi.org/10.1021/ef901105k.

11. J. Park, Z. Kang, G. Bender, M. Ulsh, and S. A. Mauger, "Roll-to-Roll Production of Catalyst Coated Membranes for Low-Temperature Electrolyzers," *Journal of Power Sources* 479 (2020): 228819, https://doi.org/10.1016/j.jpowsour.2020.228819.

12. G. Liu, S. Peng, F. Hou, X. Wang, and B. Fang, "Preparation and Performance Study of the Anodic Catalyst Layer via Doctor Blade Coating for PEM Water Electrolysis," *Membranes* 13, no. 1 (2022): 24, https://doi.org/10.3390/membranes13010024.

13. M. Koga, H. Matsumoto, M. Tokita, et al., "Investigation of Drying Process of Catalyst Ink for Polymer Electrolyte Fuel Cells by Grazing-Incidence X-Ray Scattering," *ECS Transactions* 86, no. 13 (2018): 157–161, https://doi.org/10.1149/08613.0157ecst.

14. T. Suzuki, H. Tanaka, M. Hayase, S. Tsushima, and S. Hirai, "Investigation of Porous Structure Formation of Catalyst Layers for Proton Exchange Membrane Fuel Cells and Their Effect on Cell Performance," *International Journal of Hydrogen Energy* 41, no. 44 (2016): 20326–20335, https://doi.org/10.1016/j.ijhydene.2016.09.078.

15. F. Scheepers, A. Stähler, M. Stähler, M. Carmo, W. Lehnert, and D. Stolten, "Layer Formation From Polymer Carbon-Black Dispersions," *Coatings* 8, no. 12 (2018): 450, https://doi.org/10.3390/coatings8120450.

16. F. Scheepers, A. Stähler, M. Stähler, M. Carmo, W. Lehnert, and D. Stolten, "Steering and In Situ Monitoring of Drying Phenomena During Film Fabrication," *Journal of Coatings Technology and Research* 16, no. 5 (2019): 1213–1221, https://doi.org/10.1007/s11998-019-00206-5.

17. P. Quarz, N. Zimmerer, P. Scharfer, and W. Schabel, "About Drying Phenomena of Fuel Cell and Electrolyzer CCM Inks: Selectivity of the Evaporation of 1-Propanol/Water Mixtures," *Fuel Cells* 24 (2024): fuce.202300252, https://doi.org/10.1002/fuce.202300252.

18. P. Quarz, N. Zimmerer, A.-M. Steck, P. Scharfer, and W. Schabel, "Carbon Nanotubes (CNT) as An Additive Towards Crack-Free Catalyst Coated Membranes (CCM)," *International Journal of Hydrogen Energy* 57 (2024): 789–797, https://doi.org/10.1016/j.ijhydene.2024.01.049.

19. N. Hasegawa, A. Kamiya, T. Matsunaga, N. Kitano, and M. Harada, "Analysis of Crack Formation During Fuel Cell Catalyst Ink Drying Process. Reduction of Catalyst Layer Cracking by Addition of High Boiling Point Solvent," *Colloids and Surfaces A: Physicochemical and Engineering Aspects* 628 (2021): 127153, https://doi.org/10.1016/j.colsurfa.2021.127153.

20. T. Van Cleve, G. Wang, M. Mooney, et al., "Tailoring Electrode Microstructure via Ink Content to Enable Improved Rated Power Performance for Platinum Cobalt/High Surface Area Carbon Based Polymer Electrolyte Fuel Cells," *Journal of Power Sources* 482 (2021): 228889, https://doi.org/10.1016/j.jpowsour.2020.228889.

21. A. Orfanidi, P. J. Rheinländer, N. Schulte, and H. A. Gasteiger, "Ink Solvent Dependence of the Ionomer Distribution in the Catalyst Layer of a PEMFC," *Journal of the Electrochemical Society* 165, no. 14 (2018): F1254–F1263, https://doi.org/10.1149/2.1251814jes.

22. S. Holdcroft, "Fuel Cell Catalyst Layers: A Polymer Science Perspective," *Chemistry of Materials* 26, no. 1 (2014): 381–393, https://doi.org/10.1021/cm401445h.

23. M. B. Dixit, B. A. Harkey, F. Shen, and K. B. Hatzell, "Catalyst Layer Ink Interactions That Affect Coatability," *Journal of the Electrochemical Society* 165, no. 5 (2018): F264–F271, https://doi.org/10.1149/2.0191805jes.

24. G. W. Scherer, "Theory of Drying," *Journal of the American Ceramic Society* 73, no. 1 (1990): 3–14, https://doi.org/10.1111/j.1151-2916.1990.tb05082.x.

25. T. Rieder and E. U. Schlünder, "Selective Evaporation of a Binary Mixture Into Dry or Humidified Air," *Chemical Engineering and Processing: Process Intensification* 27, no. 2 (1990): 83–93, https://doi.org/10.1016/0255-2701(90)85012-s.

26. J. Klemens, L. Schneider, E. C. Herbst, et al., "Drying of NCM Cathode Electrodes With Porous, Nanostructured Particles Versus Compact Solid Particles: Comparative Study of Binder Migration as a Function of Drying Conditions," *Energy Tech* 10, no. 4 (2022): 2100985, https://doi.org/10.1002/ente.202100985.

27. J. Kumberg, M. Müller, R. Diehm, et al., "Drying of Lithium-Ion Battery Anodes for Use in High-Energy Cells: Influence of Electrode Thickness on Drying Time, Adhesion, and Crack Formation," *Energy Tech* 7, no. 11 (2019): 1900722, https://doi.org/10.1002/ente.201900722.

28. B. Schmidt-Hansberg, H. Do, A. Colsmann, U. Lemmer, and W. Schabel, "Drying of Thin Film Polymer Solar Cells," *European Physical Journal: Special Topics* 166, no. 1 (2009): 49–53, https://doi.org/10.1140/epjst/e2009-00877-y.

29. G. Denavi, D. R. Tapia-Blácido, M. C. Añón, P. J. A. Sobral, A. N. Mauri, and F. C. Menegalli, "Effects of Drying Conditions on Some Physical Properties of Soy Protein Films," *Journal of Food Engineering* 90, no. 3 (2009): 341–349, https://doi.org/10.1016/j.jfoodeng.2008.07.001.

30. M. C. Ndukwu, L. Bennamoun, M. Simo-Tagne, M. I. Ibeh, U. C. Abada, and I. E. Ekop, "Influence of Drying Applications on Wood, Brick and Concrete Used as Building Materials: A Review," *Journal of Building Pathology and Rehabilitation* 6, no. 1 (2021): 24, https://doi.org/10.1007/s41024-021-00119-0.

31. J. Stoll, N. Zhao, X.-Z. Yuan, F. Girard, E. Kjeang, and Z. Shi, "Impacts of Cathode Catalyst Layer Defects on Performance and Durability in PEM Fuel Cells," *Journal of Power Sources* 583 (2023): 233565, https://doi.org/10.1016/j.jpowsour.2023.233565.

32. H. Liu, L. Ney, N. Zamel, and X. Li, "Effect of Catalyst Ink and Formation Process on the Multiscale Structure of Catalyst Layers in PEM Fuel Cells," *Applied Sciences* 12, no. 8 (2022): 3776, https://doi.org/10.3390/app12083776.

33. M. Kim, J.-N. Park, H. Kim, S. Song, and W.-H. Lee, "The Preparation of Pt/C Catalysts Using Various Carbon Materials for the Cathode of PEMFC," *Journal of Power Sources* 163, no. 1 (2006): 93–97, https://doi.org/10.1016/j.jpowsour.2006.05.057.

34. S. A. Berlinger, A. Chowdhury, T. Van Cleve, et al., "Impact of Platinum Primary Particle Loading on Fuel Cell Performance: Insights From Catalyst/Ionomer Ink Interactions," *ACS Applied Materials & Interfaces* 14, no. 32 (2022): 36731–36740, https://doi.org/10.1021/acsami.2c10499.

35. R. N. Bonifácio, A. O. Neto, and M. Linardi, "Influence of the Relative Volumes Between Catalyst and Nafion Ionomer in the Catalyst Layer Efficiency," *International Journal of Hydrogen Energy* 39, no. 27 (2014): 14680–14689, https://doi.org/10.1016/j.ijhydene.2014.07.004.

36. N. Kumano, K. Kudo, A. Suda, Y. Akimoto, M. Ishii, and H. Nakamura, "Controlling Cracking Formation in Fuel Cell Catalyst Layers," *Journal of Power Sources* 419 (2019): 219–228, https://doi.org/10.1016/j.jpowsour.2019.02.058.

37. S. H. Woo, S. Kim, S. Woo, et al., "Investigating the Effect of Solvent Composition on Ink Structure and Crack Formation in Polymer Electrolyte Membrane Fuel Cell Catalyst Layers," *Korean Journal of Chemical Engineering* 40, no. 10 (2023): 2455–2462, https://doi.org/10.1007/s11814-023-1474-3.

38. C. M. Cardinal, Y. D. Jung, K. H. Ahn, and L. F. Francis, "Drying Regime Maps for Particulate Coatings," *AIChE Journal* 56, no. 11 (2010): 2769–2780, https://doi.org/10.1002/aic.12190.

39. S. Jaiser, J. Kumberg, J. Klaver, et al., "Microstructure Formation of Lithium-Ion Battery Electrodes During Drying—An Ex-Situ Study Using Cryogenic Broad Ion Beam Slope-Cutting and Scanning Electron Microscopy (Cryo-BIB-SEM)," *Journal of Power Sources* 345 (2017): 97–107, https://doi.org/10.1016/j.jpowsour.2017.01.117.

40. K. B. Singh and M. S. Tirumkudulu, "Cracking in Drying Colloidal Films," *Physical Review Letter* 98, no. 21 (2007): 218302, https://doi.org/10.1103/PhysRevLett.98.218302.

41. A. F. Routh, "Drying of Thin Colloidal Films," *Reports on Progress in Physics* 76, no. 4 (2013): 046603, https://doi.org/10.1088/0034-4885/76/4/046603.

42. S. Kundu, M. W. Fowler, L. C. Simon, and S. Grot, "Morphological Features (Defects) in Fuel Cell Membrane Electrode Assemblies," *Journal of Power Sources* 157, no. 2 (2006): 650–656, https://doi.org/10.1016/j.jpowsour.2005.12.027.

43. W. Wang, S. Chen, J. Li, and W. Wang, "Fabrication of Catalyst Coated Membrane With Screen Printing Method in a Proton Exchange Membrane Fuel Cell," *International Journal of Hydrogen Energy* 40, no. 13 (2015): 4649–4658, https://doi.org/10.1016/j.ijhydene.2015.02.027.

44. T. Riede and E. U. Schlünder, "Evaporation and Pervaporation of a Binary Mixture From an Inert Carrier Liquid," *Chemical Engineering & Technology* 11, no. 1 (1988): 384–391, https://doi.org/10.1002/ceat.270110150.

45. P. Quarz, L. Janning, N. Zimmerer, P. Scharfer, and W. Schabel, "Selective Evaporation of Solvent Mixtures in Thin Films for Fuel Cell and Electrolyser Catalyst Coatings," *Drying Technology* 44 (2026): 346–355, https://doi.org/10.1080/07373937.2026.2616748.

46. N. Zimmerer, P. Quarz, E. Terhorst, L. Janning, P. Scharfer, and W. Schabel, *Energy Technology* 13, no. 12 (2025): 2500516, https://doi.org/10.1002/ente.202500516.

47. T. Mabuchi, S.-F. Huang, and T. Tokumasu, "Dispersion of Nafion Ionomer Aggregates in 1-Propanol/Water Solutions: Effects of Ionomer Concentration, Alcohol Content, and Salt Addition," *Macromolecules* 53, no. 9 (2020): 3273–3283, https://doi.org/10.1021/acs.macromol.9b02725.

48. S. Khandavalli, J. H. Park, H. H. Winter, D. J. Myers, M. Ulsh, and S. A. Mauger, "Viscoelasticity Enhancement and Shear Thickening of Perfluorinated Sulfonic Acid Ionomer Dispersions in Water–Alcohol Solvent Mixtures," *Macromolecules* 56, no. 17 (2023): 6988–7005, https://doi.org/10.1021/acs.macromol.3c00383.

49. S. A. Berlinger, B. D. McCloskey, and A. Z. Weber, "Inherent Acidity of Perfluorosulfonic Acid Ionomer Dispersions and Implications for Ink Aggregation," *Journal of Physical Chemistry B* no. 31 (2018): 7790–7796, https://doi.org/10.1021/acs.jpcb.8b06493.

50. N. Zimmerer, P. Quarz, L. Janning, P. Scharfer, and W. Schabel, "In-Situ Investigation of Crack Formation During Drying of Catalyst Layers for Polymer Electrolyte Membrane (PEM) Fuel Cells and Electrolyzer," *Colloids and Surfaces A: Physicochemical and Engineering Aspects* 728 (2026): 138807, https://doi.org/10.1016/j.colsurfa.2025.138807.

51. M. Baunach, S. Jaiser, S. Schmelzle, H. Nirschl, P. Scharfer, and W. Schabel, "Delamination Behavior of Lithium-Ion Battery Anodes: Influence of Drying Temperature During Electrode Processing," *Drying Technology* 34, no. 4 (2016): 462–473, https://doi.org/10.1080/07373937.2015.1060497.

52. S. Jaiser, A. Friske, M. Baunach, P. Scharfer, and W. Schabel, "Development of a Three-Stage Drying Profile Based on Characteristic Drying Stages for Lithium-Ion Battery Anodes," *Drying Technology* 35, no. 10 (2017): 1266–1275, https://doi.org/10.1080/07373937.2016.1248975.

53. B. Schmidt-Hansberg, M. Baunach, J. Krenn, et al., "Spatially Resolved Drying Kinetics of Multi-Component Solution Cast Films for Organic Electronics," *Chemical Engineering and Processing: Process Intensification* 50, no. 5–6 (2011): 509–515, https://doi.org/10.1016/j.cep.2010.12.012.

54. M. B. Satterfield and J. B. Benziger, "Viscoelastic Properties of Nafion at Elevated Temperature and Humidity," *Journal of Polymer Science: Polymer Physics* 47, no. 1 (2009): 11–24, https://doi.org/10.1002/polb.21608.

55. M. Ozmaian and R. Naghdabadi, "Properties of Nafion Under Uniaxial Loading at Different Temperatures: A Molecular Dynamics Study," *Polymer-Plastics Technology and Engineering* 54, no. 8 (2015): 806–813, https://doi.org/10.1080/03602559.2014.974192.

56. M. Yamamura, "Manipulating Cracks With Selective Drying in Binary Solvent Mixture Suspensions," *Journal of Chemical Engineering of Japan* 58, no. 1 (2025): 2545622, https://doi.org/10.1080/00219592.2025.2545622.

Supporting Information

Additional supporting information can be found online in the Supporting Information section.

This section includes additional experimental results backing up the findings from this work.

Supporting File: ceat70192-sup-0001-SuppMat.docx.